Formation of surface defects by thermal shock method for the improved photocatalytic activity of ZnO nanoparticles

Le, Tien Khoa; Nguyen, The Luan; Hoang, Chau Ngoc; Nguyen, Dieu Khanh An; Lund, Torben; Nguyen, Huu Khanh Hung; Huynh, Thi Kieu Xuan

Published in:
Journal of Asian Ceramic Societies

DOI:
10.1080/21870764.2020.1720900

Publication date:
2020

Document Version
Publisher's PDF, also known as Version of record

Citation for published version (APA):
Le, T. K., Nguyen, T. L., Hoang, C. N., Nguyen, D. K. A., Lund, T., Nguyen, H. K. H., & Huynh, T. K. X. (2020). Formation of surface defects by thermal shock method for the improved photocatalytic activity of ZnO nanoparticles. *Journal of Asian Ceramic Societies*, *8*(1), 193-202. https://doi.org/10.1080/21870764.2020.1720900

Journal of Asian Ceramic Societies

ISSN: (Print) 2187-0764 (Online) Journal homepage: https://www.tandfonline.com/loi/tace20

Formation of surface defects by thermal shock method for the improved photocatalytic activity of ZnO nanoparticles

Tien Khoa Le, The Luan Nguyen, Chau Ngoc Hoang, Dieu Khanh An Nguyen, Torben Lund, Huu Khanh Hung Nguyen & Thi Kieu Xuan Huynh

To cite this article: Tien Khoa Le, The Luan Nguyen, Chau Ngoc Hoang, Dieu Khanh An Nguyen, Torben Lund, Huu Khanh Hung Nguyen & Thi Kieu Xuan Huynh (2020) Formation of surface defects by thermal shock method for the improved photocatalytic activity of ZnO nanoparticles, Journal of Asian Ceramic Societies, 8:1, 193-202, DOI: 10.1080/21870764.2020.1720900

To link to this article: https://doi.org/10.1080/21870764.2020.1720900

Published online: 30 Jan 2020.

JOURNAL OF ASIAN CERAMIC SOCIETIES
2020, VOL. 8, NO. 1, 193–202
https://doi.org/10.1080/21870764.2020.1720900

THE CERAMIC SOCIETY OF JAPAN
THE KOREAN CERAMIC SOCIETY
Taylor & Francis
Taylor & Francis Group

FULL LENGTH ARTICLE

Formation of surface defects by thermal shock method for the improved photocatalytic activity of ZnO nanoparticles

Tien Khoa Le[a], The Luan Nguyen[a], Chau Ngoc Hoang[a], Dieu Khanh An Nguyen[b], Torben Lund[c], Huu Khanh Hung Nguyen[a] and Thi Kieu Xuan Huynh[a]

[a]Department of Chemistry, VNUHCM - University of Science, Ho Chi Minh, Vietnam; [b]Faculty of Chemistry, University of Strasbourg, Strasbourg, France; [c]Department of Science and Environment, Roskilde University, Roskilde, Denmark

ABSTRACT

Surface-modified ZnO photocatalysts with enhanced UVA-light-driven and visible-light-driven activities were synthesized by the thermal shock method with $Cu(NO_3)_2$ at different thermal shock temperatures (300 – 600°C). The influences of thermal shock temperatures on the crystal structure, morphology, surface functional groups and surface composition of modified catalysts were investigated by XRD, TEM, Raman and XPS spectra, respectively. Their photocatalytic activity was evaluated via the degradation of methylene blue under both UVA and visible light irradiation. According to the results, by combining the thermal shock method and an agent with low thermal stability such as $Cu(NO_3)_2$, we did not modify the crystal structure, phase composition nor the morphology of ZnO nanoparticles, but successfully modified the surface of ZnO nanoparticles with the migration of zinc ions, leading to the creation of new environments of Zn^{2+} and O^{2-} ions as well as the formation of surface zinc vacancies. These evolutions were found to be able to enhance the photocatalytic performance in the UVA light region and also in the visible light region.

ARTICLE HISTORY
Received 26 November 2019
Accepted 21 January 2020

KEYWORDS
ZnO; photocatalysis; surface modification; thermal shock; surface zinc vacancies

1. Introduction

Over the past decades, photocatalysis based on the performance of various transition metal oxides like ZnO has been considered as one of the most promising methods for water treatment [1–4]. However, the recombination of photogenerated electrons-holes which occurs during the photocatalytic process as well as the possibility to operate under UV light irradiation due to the large bandgap are the main reasons limiting the applications of ZnO in industrial scale. Therefore, a wide range of studies have been carried out to modify the oxide with nonmetal or transition metal ions. Recently, several works revealed that the creation of intrinsic or extrinsic defects such as oxygen vacancies, zinc vacancies, zinc interstitials and impurities can help to effectively control the photocatalytic performance of ZnO. Specifically, the presence of these defects can improve or decline the oxide activity, depending on the type and the position of defects [5–8]. According to the work of Chen et al. [9], when the oxygen vacancies or zinc vacancies are formed in the bulk structure of ZnO, they can act as the recombination centers of photogenerated charges, preventing the transport of photogenerated electrons and holes to the surface and consequently their reactions with adsorbed species. Likewise, by using a simple ball-milling technique, Aggelopoulos et al. successfully created the oxygen vacancies in ZnO lattice and observed the systematic decrease in photocatalytic activity when the milling time increased [10].

By contrast, the formation of different defects on the surface of ZnO has been recognized as a potential way to ameliorate its photocatalytic response. In fact, by using the ZnO_2 precursor, Wang et al. successfully synthesized ZnO nanoparticles with a high concentration of oxygen vacancies on the material surface [11]. These surface oxygen vacancies are supposed to create an intermediate energy level near the valence band of this oxide, which induces the bandgap narrowing and resultantly the photocatalytic performance in the visible light region [12,13]. Moreover, the surface oxygen vacancies were also proved to behave as electron traps, promoting the separation of photogenerated electrons-holes and thereby effectively improving the photocatalytic activity [14,15]. Similar to oxygen vacancies, it was reported that the surface zinc vacancies can also create impurity energy levels in the bandgap of ZnO [16]. As a result, the ZnO photocatalysts with surface zinc vacancies are capable of absorbing the visible light and resulting in the visible-light-induced activity.

Nevertheless, in order to create the surface defects, ZnO was usually prepared and treated by complicated procedures (atomic layer deposition [17], hydrothermal process [18] or vacuum deoxidation [13]) with expensive chemicals (ZnO_2 [11], $NaBH_4$ [15]). Recently, we developed the thermal shock technique, a simple, easy-to-implement method which is based

CONTACT Thi Kieu Xuan Huynh htkxuan@hcmus.edu.vn Department of Chemistry, VNUHCM - University of Science, 227 Nguyen Van Cu Street, Dist.5, Ho Chi Minh, Vietnam

on the thermal treatment of a material during a short time [19,20]. Different from the combustion synthesis method relying on a thermally induced redox reaction between an oxidant and a fuel [21–24], the thermal shock method is simply an abrupt temperature change of a solid material with appropriate precursors at some high temperatures during a short time, which allows us to forcefully modify the surface of this material without affecting its bulk structure. In fact, due to the short heating time (only 5 min), the modifications caused by thermal shock are likely to be limited to the surface with the formation of surface defects. Since most of the photocatalytic reactions occur on the surface of a heterogeneous semiconductor, this modification method is found to be very suitable for the performance control of photocatalysts. Moreover, in order to create a great number of surface defects, we assume that it is necessary to use the precursors which can be thermally decomposed during the thermal shock, thereby creating disturbances on the sample surface. Therefore, in this work, we suggest to modify ZnO nanoparticles by using the thermal shock technique with $Cu(NO_3)_2$ precursor. Since $Cu(NO_3)_2$ is a compound that can be decomposed and produce gas at low temperature, we believe that using this precursor during the thermal shock method is a promising way to improve the photocatalytic activity of ZnO under both UVA and visible light illumination. The influences of thermal shock with $Cu(NO_3)_2$ precursor at different temperatures on the crystal structure, surface morphology and surface composition of ZnO were also investigated and discussed in detail.

2. Materials and methods

2.1. Catalyst preparation and modification

In this study, the precursors $Zn(CH_3COO)_2.2H_2O$, $Cu(NO_3)_2.2.5H_2O$ (>98%, ACS reagent) and $H_2C_2O_4.2H_2O$ (>99%, ACS reagent) were purchased from Sigma Aldrich (USA). Methylene blue (MB, analytical grade) was also purchased from Sigma Aldrich (USA). All chemicals were used as received without further purification. Distilled deionized water was used in all experimental work.

In the first stage, ZnO nanoparticles were prepared by a simple precipitation-annealing method. Briefly, 0.5 $mol.L^{-1}$ $Zn(CH_3COO)_2$ solution was added to $H_2C_2O_4$ solution (0.5 $mol.L^{-1}$), magnetically stirred at room temperature during 1 h to obtain a white precipitate. This precipitate was thoroughly washed with deionized water until there is no more ion detected in the filtrate (using conductimetry tests). Then, the precipitate was dried at 120°C for 1 h and subsequently heated at 500°C for 2 h to produce ZnO nanoparticles.

In the second stage, the as-prepared ZnO nanoparticles were surface-modified by thermal shock method with $Cu(NO_3)_2$ precursor at different temperatures. First of all, $Cu(NO_3)_2$ solution was poured into the beaker containing ZnO powder to reach the molar ratio of Zn: Cu fixed at 1:0.005. The mixture was regularly stirred for 20 min to well distribute $Cu(NO_3)_2$ to the surface of ZnO nanoparticles and dried at 150°C during 3 h. Next, the thermal shock for 5 min was carried out by putting the obtained powder into the Nabertherm muffle furnace (maximum 9 kW) preheated at different temperatures (300°C, 400°C, 500°C and 600°C with a heating rate of 1° $C.min^{-1}$). After 5 min, the powder samples were immediately removed from the furnace and cooled in an ambient atmosphere to room temperature. Finally, the products were washed with distilled deionized water, dried at 150°C for 1 h in order to remove nitrate species from the ZnO surface. In the following manuscript, the ZnO samples surface-modified with $Cu(NO_3)_2$ by thermal shock were labeled as mod-ZnO-X (with X the thermal shock temperature). The ZnO sample modified only by thermal shock without $Cu(NO_3)_2$ was also prepared by the same procedure (thermal shock temperature of 300°C) and denoted as TS-ZnO.

2.2. Characterization

The crystal structure and the phase composition of unmodified ZnO and surface-modified ZnO samples at different thermal shock temperatures were investigated by the powder X-ray diffraction on a BRUKER-Binary V3 X-ray diffractometer equipped with a Cu Kα source (λ = 1.5406 Å). The accelerating voltage and the applied current were fixed to 40 kV and 40 mA, respectively. The scanning rate was held constant at 0.019° s^{-1}. In order to characterize the surface morphology of catalysts, the TEM (transmission electron microscopy) images were captured on a JEOL JEM-1400 system at the accelerating voltage of 100 kV.

The Raman spectroscopy was used to investigate the vibrations of chemical bonds on the surface of catalysts. The Raman spectra were taken by a HORIBA Jobin-Yvon spectrophotometer consisting of diode pumped solid-state laser with 532 nm wavelength.

Besides, the surface atomic composition and chemical environment of unmodified ZnO and surface-modified ZnO samples were also studied by X-ray photoelectron spectroscopy (XPS) on a Kratos Axis Ultra DLD spectrometer (Kratos Analytical Ltd, UK) using the Al-Kα source (1486.6 eV) and the pressure of 10^{-7} mbar. All binding energies of elements in different chemical environments on the surface of catalysts were referenced to the C1s line at 285 eV, corresponding to the surface contamination carbon. The Rietveld refinement was carried out by using the Fullprof 2009 structure refinement software [25].

2.3. Catalytic tests

The photocatalytic performance of unmodified ZnO and surface-modified ZnO samples was examined via the MB degradation under UVA light and visible light illumination. In a typical photocatalytic test, 250 mL of MB solution (10^{-5} mol.L^{-1}) was mixed with 0.125 g catalyst powder in a glass beaker under continuous stirring. The initial pH of suspensions was determined at 7. An Osram 9-W UV light lamp and an Osram 9-W visible light lamp were used for the irradiation in UVA and visible light region, respectively. These lamps were placed about 10 cm above the suspension surface. Before the lamps were turned on, the suspension was vigorously stirred in the dark for 60 min to ensure the adsorption-desorption equilibrium of MB aqueous solution with the photocatalysts. Then, the solution containing MB and catalysts was exposed to the UVA light or visible light for a certain period of time. A water circulation system was used to maintain the reactor temperature at 30°C during the experiments. In order to monitor the progress of MB degradation, the absorbance of MB at 664 nm was measured at regular time intervals by a UV-visible Helios Omega spectrophotometer.

3. Results and discussion

3.1. Crystal structures and morphology

In order to investigate the impacts of thermal shock modification on the crystal structure, phase composition and surface morphology, the unmodified ZnO, TS-ZnO and mod-ZnO catalysts were, respectively, characterized by powder XRD and TEM techniques. The XRD patterns of all samples (Figure 1) exhibit the intense and symmetrical diffraction peaks at 31.82°, 34.41°, 36.22°, 47.60°, etc., which are characteristic of ZnO zincite phase (space group P63mc, JCPDS file no. 36–1451) in well-crystallized states. Moreover, no impurity phase was observed in these patterns. Likewise, the TEM images of all samples show the same morphology, with polyhedral particles in the size distribution from 20 to 100 nm (Figure 2). These results demonstrate that the thermal shock process with $Cu(NO_3)_2$ at different temperatures did not modify the phase composition, crystal structure and the particle size of ZnO nanoparticles.

3.2. Surface characterization

As mentioned above, in this study, we focused on studying the surface modification of ZnO nanoparticles by thermal shock method with $Cu(NO_3)_2$. Figure 3 shows the Raman spectra of three samples ZnO, mod-ZnO-300 and mod-ZnO-500. The unmodified ZnO sample presents two peaks with high intensity, situated at 96.28 and 437.84 cm^{-1}, which are featured for ZnO wurtzite phase [26,27]. The former peak is attributed to the E_2(low) vibration mode of zinc ions while the latter peak belongs to the E_2(high) vibration mode of oxygen ions on the oxide surface. In addition, a weak peak was observed at 330.84 cm^{-1} in the Raman spectrum of unmodified ZnO sample, corresponding to the second-order scattering processes of E_2(high)-E_2(low) multi-phonon mode [28,29]. When ZnO was modified with $Cu(NO_3)_2$ by thermal shock method at different temperatures, the Raman spectra still present these three characteristic peaks, but the intensity of the peaks associated with E_2(low) and E_2(high) modes dramatically decreases. Moreover, in the Raman spectra of surface-modified catalysts, the E_2(high) peak is found to be shifted to the lower wavenumber. These

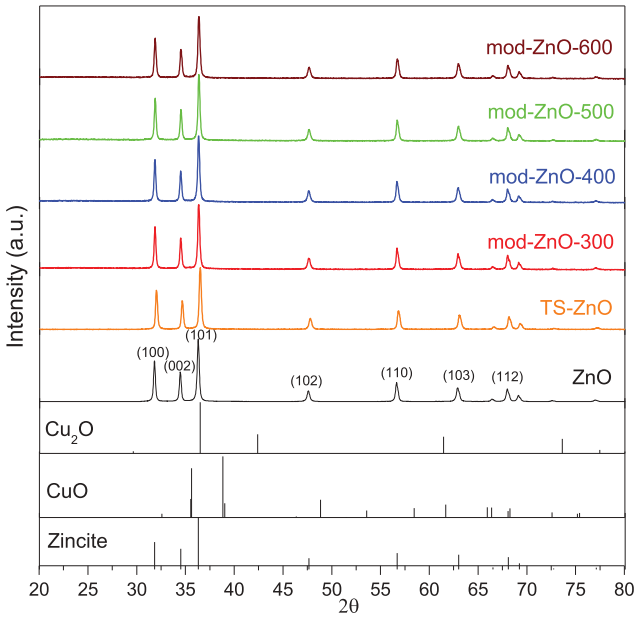

Figure 1. XRD patterns of unmodified ZnO, thermal-shock-modified ZnO without $Cu(NO_3)_2$ and thermal-shock-modified ZnO samples with $Cu(NO_3)_2$ at different thermal shock temperatures.

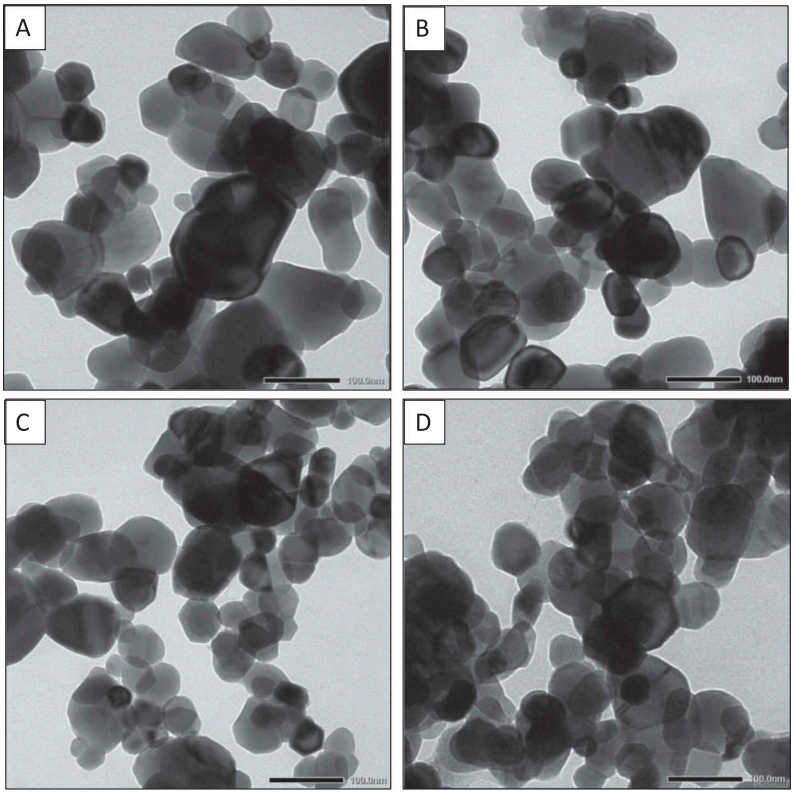

Figure 2. TEM images of (a) unmodified ZnO, (b) mod-ZnO-300, (c) mod-ZnO-500 and (d) mod-ZnO-600 samples.

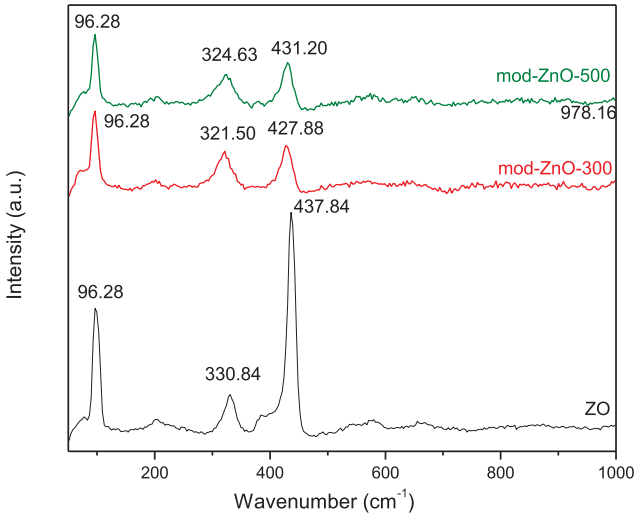

Figure 3. Raman spectra of unmodified and thermal-shock-modified ZnO samples with $Cu(NO_3)_2$ (mod-ZnO-300 and mod-ZnO-500).

changes reveal that the thermal shock with $Cu(NO_3)_2$ affected the Zn-O bonds on the catalyst surface, which can lead to disturbances of zinc and oxygen ions or the formation of intrinsic defects on the surface of ZnO nanoparticles.

Therefore, in order to elucidate the influences of thermal-shock modification on the surface composition and chemical environment of atoms on the surface, all our catalysts were analyzed by XPS, a specific method for surface characterization of solid materials. The XPS results are summarized in Table 1. Figure 4 presents the high-resolution Zn 2p spectra of unmodified ZnO, TS-ZnO, mod-ZnO-300 and mod-ZnO-500 samples. For unmodified ZnO catalyst, the Zn $2p_{3/2}$ and $2p_{1/2}$ spin-orbit peaks are observed at 1021.4 and 1044.5 eV, respectively, corresponding to the binding energies of Zn^{2+} ions in ZnO lattice [30,31]. When ZnO was surface-modified at 300°C without $Cu(NO_3)_2$, the position and the shape of these peaks were not altered. However, when ZnO was surface-modified at 300°C with $Cu(NO_3)_2$, the Zn 2p peaks became asymmetrical, indicating the evolution in composition and

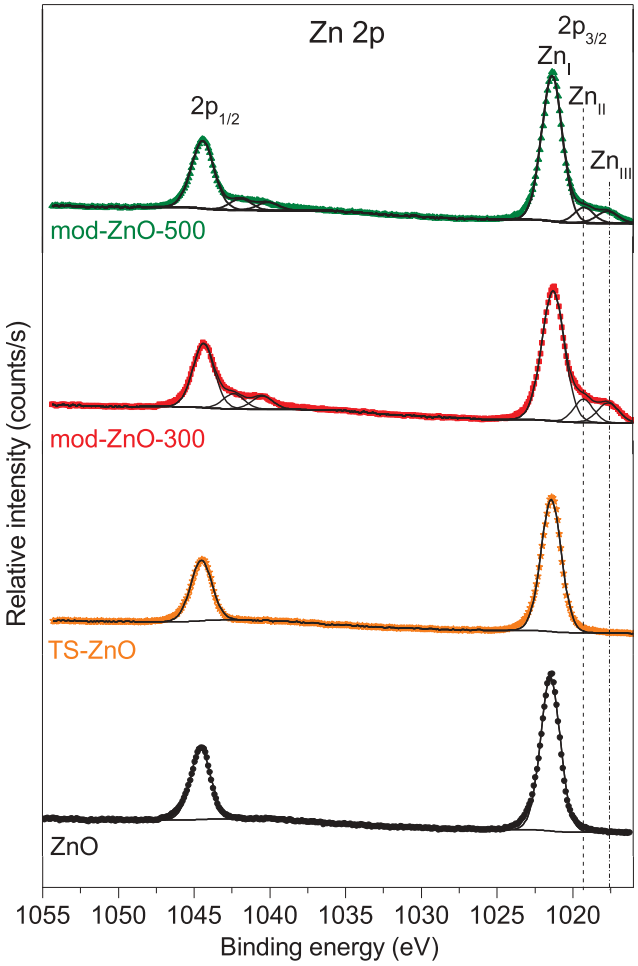

Figure 4. High-resolution XPS Zn 2p spectra of unmodified ZnO, TS-ZnO, mod-ZnO-300 and mod-ZnO-500 samples.

Table 1. High-resolution XPS data of unmodified ZnO, TS-ZnO, mod-ZnO-300 and mod-ZnO-500 samples.

		C 1s			Zn $2p_{3/2\text{-}1/2}$ I	Zn $2p_{3/2\text{-}1/2}$ II	Zn $2p_{3/2\text{-}1/2}$ III	O 1s I	O 1s II	O 1s III	O 1s IV
ZnO	B.E. eV	285.0	286.6	289.0	1021.4–1044.5			530.2	531.8		
	%	13.00	1.94	2.38	34.32			34.33	14.03		
TS-ZnO	B.E. eV	285.0	286.6	288.8	1021.4–1044.5			530.2	531.8		
	%	14.30	2.11	2.51	33.97			33.81	13.30		
mod-ZnO-300	B.E. eV	285.0	286.5	288.8	1021.2–1044.3	1019.3–1042.4	1017.6–1040.5	530.2	531.8	528.5	526.4
	%	16.04	1.41	1.53	23.74	4.30	3.94	29.11	10.75	5.13	4.06
mod-ZnO-500	B.E. eV	285.0	286.8	289.1	1021.4–1044.4	1019.2–1041.9	1017.7–1040.1	530.2	531.8	528.7	527.1
	%	14.45	5.32	2.09	25.06	3.06	2.43	30.56	11.23	2.97	2.28

chemical environment of zinc ions on the surface. For this sample, the Zn 2p peaks can be deconvoluted into 3 components: the main components (Zn_I) situated at 1021.3 (Zn $2p_{3/2}$) and 1044.4 eV (Zn $2p_{1/2}$), characteristic of Zn^{2+} ions in ZnO lattice [30,31] and two other spin-orbit components with lower intensity at 1019.2–1042.3 eV (Zn_{II}) and 1017.6–1040.4 (Zn_{III}). Since their binding energies are lower than that of Zn^{2+} in ZnO lattice, the new minor components can be attributed to the zinc ions less oxidized or zinc ions in oxygen-deficient regions. However, when the thermal shock temperature was up to 500°C, the intensity of these components decreased, indicating the declined content of Zn^{2+} ions in the new chemical environments.

Figure 5 presents the O 1s XPS spectra of unmodified ZnO, TS-ZnO, mod-ZnO-300 and mod-ZnO-500 samples. It was observed that the O 1s core peaks of both four samples are asymmetric and comprise more than one component. For unmodified ZnO and TS-ZnO samples, the core peaks O 1s can be deconvoluted into two components: the main and intense component (O_I) at 530.2 eV assigned to O^{2-} ions in ZnO lattice [32] whereas the weak component at 531.8 eV attributed to surface hydroxyl groups [33]. However, the XPS O 1s spectra of mod-ZnO-300 and mod-ZnO-500 samples are more complicated. In addition to O_I and O_{II} components, the O 1s peaks of mod-ZnO-300 catalyst also contain two new components at lower binding energies: 528.4 (O_{III}) and 526.4 eV (O_{IV}). This is very interesting because, according to our best understanding, there seems to be no report about oxygen environments having lower binding energy than that of O^{2-}

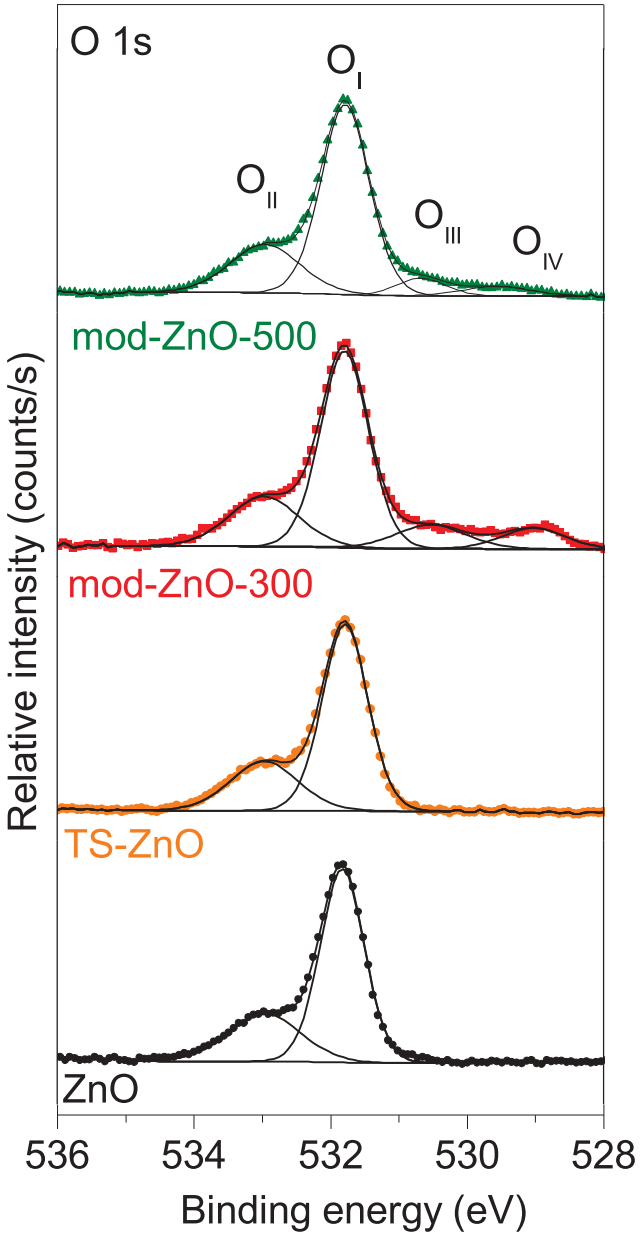

Figure 5. High-resolution XPS O 1s spectra of unmodified ZnO, TS-ZnO, mod-ZnO-300 and mod-ZnO-500 samples.

Table 2. Comparison of atomic ratios calculated from corresponding XPS peak area of unmodified ZnO, TS-ZnO, mod-ZnO -300 and mod-ZnO-500 samples.

Sample		ZnO	TS-ZnO	mod-ZnO -300	mod-ZnO -500
Atomic ratios calculated from corresponding XPS peak area	$(Zn_I + Zn_{II} + Zn_{III})/(O_I + O_{III} + O_{IV})$	1.00	1.00	0.83	0.85
	$O_{II}/(Zn_I + Zn_{II} + Zn_{III})$	0.41	0.40	0.34	0.37

ions in the lattice of ZnO. It is possible that the new O 1s components belong to the O^{2-} ions located in the zinc-excessive regions, which may be created by the thermal shock process. Similar to the XPS Zn 2p spectra, we also observed that the intensity of new O 1s components (O_{III} and O_{IV}) tends to decrease when ZnO nanoparticles were modified at the thermal-shock temperature of 500°C.

In our XPS study, the molar Zn^{2+}/O^{2-} ratios as well as the molar OH/Zn^{2+} ratios were calculated using the corresponding peak areas $((Zn_I + Zn_{II} + Zn_{III})/(O_I + O_{III} + O_{IV})$ and $O_{II}/(Zn_I + Zn_{II} + Zn_{III})$. According to Table 2, the unmodified ZnO and TS-ZnO samples show the molar Zn^{2+}/O^{2-} ratio of 1/1, which is consistent with the stoichiometric ratio of elements in ZnO. However, for mod-ZnO-300 and mod-ZnO-500 samples, this molar ratio greatly decreased, indicating the zinc-deficiencies on their surfaces. The zinc-deficiencies are likely to correspond to the formation of zinc vacancies on ZnO surface after the thermal-shock modification. Moreover, the content of surface hydroxyl groups of ZnO powders modified with $Cu(NO_3)_2$ also tends to decline. It should

be noted that when we changed the thermal shock temperature from 500°C to 300°C, the evolution of elemental composition and chemical environments on the catalyst surface became stronger, which was proved by the further decrease in molar Zn^{2+}/O^{2-} ratio (from 0.868 to 0.835) and the further increase in the content of new components of surface zinc and oxygen ions. This suggests that the thermal shock at 300°C affects the surface of ZnO nanoparticles more than that at 500°C. Besides, we do not detect any copper species on the surface of modified ZnO samples, indicating that the content of copper species may be below the detection limit of XPS technique. All these results demonstrate that using $Cu(NO_3)_2$ allows us to effectively modify the surface of ZnO, creating the disturbance in chemical environments of Zn^{2+} and O^{2-} ions without leaving impurities on the surface.

3.3. Photocatalytic activity

Figure 6 and 7 compare the MB degradation over different photocatalysts under UVA light (Figure 6) and visible light (Figure 7). It was observed that the photocatalytic MB degradation always followed the pseudo-first-order Langmuir–Hinshelwood kinetic model, which allows us to evaluate the performance of our photocatalysts via their apparent rate constants k (Table 3). Under UVA and visible light, the rate constant of MB degradation in the presence of unmodified ZnO was found to be 3.20 and 0.17 h^{-1}, respectively. These rate constants remained practically

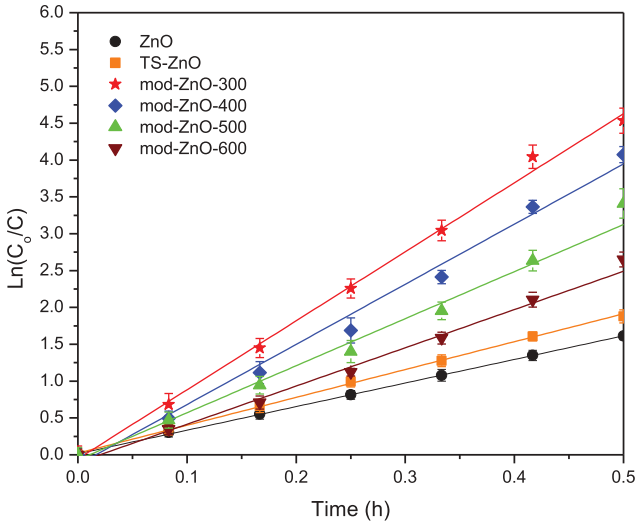

Figure 6. Ln(C_0/C) versus time plot of MB degradation under UV irradiation on unmodified ZnO, thermal-shock-modified ZnO without $Cu(NO_3)_2$ and thermal-shock-modified ZnO samples with $Cu(NO_3)_2$. C is the MB concentration (mol.L^{-1}) at time t and C_0 is the initial MB concentration (mol.L^{-1}).

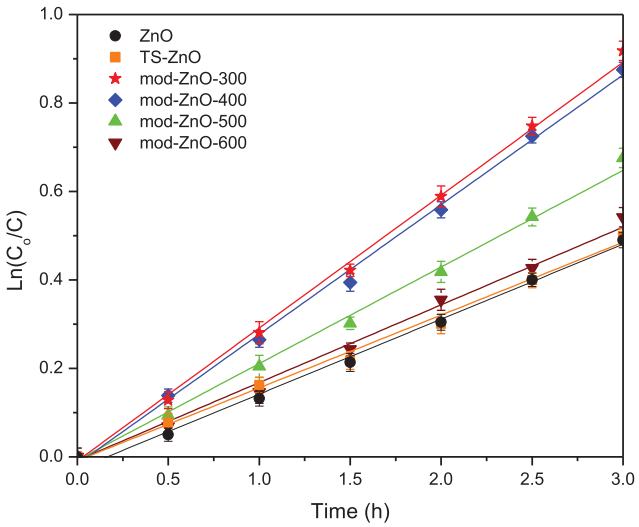

Figure 7. Ln(C_0/C) versus time plot of MB degradation under visible irradiation on unmodified ZnO, thermal-shock-modified ZnO without $Cu(NO_3)_2$ and thermal-shock-modified ZnO samples with $Cu(NO_3)_2$. C is the MB concentration (mol.L^{-1}) at time t and C_0 is the initial MB concentration (mol.L^{-1}).

Table 3. Comparison of MB degradation rate constant on unmodified ZnO, thermal-shock-modified ZnO without $Cu(NO_3)_2$ and thermal-shock-modified ZnO samples with $Cu(NO_3)_2$ under UVA and visible light irradiation.

Sample		ZnO	TS-ZnO	mod-ZnO -300	mod-ZnO -400	mod-ZnO -500	mod-ZnO -600
Apparent rate constant (k_{app}) of MB degradation (h^{-1})	Under UVA light illimunation	3.20	3.71	9.44	8.32	6.94	5.32
	Under visible light illumination	0.17	0.17	0.31	0.29	0.22	0.18

unchanged for TS-ZnO sample. But when ZnO was modified with $Cu(NO_3)_2$ by thermal shock method at 300°C, the photocatalytic activity was greatly enhanced. In fact, the rate constant of MB degradation using mod-ZnO-300 sample was nearly 3 times (under UVA light) and 2 times (under visible light) higher than those using unmodified ZnO sample. However, further increase of the thermal shock temperature (from 300°C to 600°C) resulted in a gradual decrease in photocatalytic performance. Under UVA light or visible light, the mod-ZnO-600 only exhibited the rate constant of 5.32 h^{-1} and 0.18 h^{-1}, respectively. These results depict that the thermal shock temperature plays an important role for the performance of photocatalysts. Among all samples, the mod-ZnO-300 was found to be the best photocatalyst under both UVA light and visible light.

3.4. Discussion

The experimental results demonstrated that the thermal shock method with or without $Cu(NO_3)_2$ barely lead to any modification in the crystal structure, phase composition and morphology of ZnO nanoparticles. However, in the presence of $Cu(NO_3)_2$, the thermal shock can induce various changes in the chemical composition and environments on the surface of ZnO. It should be reminded that all mod-ZnO samples depicted higher photocatalytic activity under both UVA light and visible light than ZnO and TS-ZnO samples. Therefore, the enhanced performance of mod-ZnO catalysts is most likely due to the surface modifications after the thermal shock process.

In fact, when ZnO was thermal-shock-modified with $Cu(NO_3)_2$ at 300°C, the XPS study indicated many changes on the material surface, including the formation of new environments of Zn^{2+} and O^{2-} ions, the decrease in surface hydroxyl groups and the formation of surface zinc vacancies. Specifically, on the surface of mod-ZnO -300, Zn^{2+} ions are not only situated in the chemical environment of ZnO, but also located in the environment less oxidized than ZnO or in the oxygen-deficient regions. Likewise, a number of O^{2-} ions were also found in the zinc-excessive regions. These evolutions were not clearly observed in the TS-ZnO sample, proving the vital role of $Cu(NO_3)_2$ for the surface modification of ZnO nanoparticles. It should be noted that before the thermal shock process, ZnO nanoparticles were mixed in $Cu(NO_3)_2$ solution. Owing to this step, all the surfaces of ZnO nanoparticles were covered by $Cu(NO_3)_2$. Since $Cu(NO_3)_2$ can be decomposed at low temperature (263°C [34]), in the next step, the thermal shock at 300°C possibly induced the thermal decomposition of $Cu(NO_3)_2$, which causes numerous disturbances on the surface of ZnO, including the migration of Zn^{2+} ions. Due to their small radius, a portion of Zn^{2+} ions can leave their balance positions to move to the interstitial sites, consequently forming at the same time zinc vacancies and new chemical environments where Zn^{2+} ions are less oxidized and O^{2-} ions are connected to Zn^{2+} ions more than the conventional environment of O^{2-} ions in ZnO. Moreover, the interstitial Zn^{2+} ions can interact with surface hydroxyl groups, convert the Zn-O-H bonds to Zn-O-Zn bonds. Hence, the surface hydroxyl groups tend to decrease on the surface of mod-ZnO samples.

Previously, many studies reported that the enhanced photocatalytic activity can be obtained by increasing the surface hydroxyl groups [35,36]. Nevertheless, in this work, the photocatalytic performance of our catalysts was effectively improved despite the decrease in surface hydroxyl groups, which indicates that the content of surface hydroxyl groups is not the main factor determining the activity. In contrast, according to several recent studies, surface zinc vacancies have been considered as a positive factor that can contribute to the enhancement of photocatalytic activity. Through DFT calculations, Pan et al. successfully proved that the formation of zinc vacancies is able to create the intermediate energy level in the bandgap, above the valence band of ZnO [16]. Owing to these intermediate levels, the electrons in the ZnO valence band require less energy to move to the conduction band, which hinders the recombination of electron-hole pairs, promotes the visible-light-absorption, then improves the photocatalytic performance under both UVA light and visible light. This argument is further reinforced through the bandgap values of ZnO and mod-ZnO-300 samples measured by the UV-Visible diffuse reflectance spectra which were recorded at room temperature on a Perkin–Elmer Lambda 850 Spectrophotometer. Accordingly, the bandgap value of mod-ZnO-300 (2.87 eV) is found to be lower than that of unmodified ZnO (3.19 eV), which demonstrated the impact of surface zinc vacancies on the optical properties of ZnO nanoparticles. However, when the thermal shock temperature overpassed 300°C, the quantity of Zn^{2+} and O^{2-} ions in the new chemical environments as well as the content of surface zinc vacancies gradually decreased. It seems that at thermal shock temperatures above 300°C, $Cu(NO_3)_2$ decomposes too quickly, which reduces the

impacts of modification on the oxide surface thus declines the photocatalytic activity. This problem needs to be further clarified in our future studies.

4. Conclusion

In this work, by using the thermal shock method with $Cu(NO_3)_2$ agent at different temperatures, we successfully modified the surface of ZnO nanoparticles without affecting their crystal structure, phase composition and morphology. All surface-modified ZnO samples exhibitedan enhanced photocatalytic activity under both UVA light and visible light. This improvement of activity can be explained by the impacts of thermal shock with $Cu(NO_3)_2$, which promotes the migration of zinc ions and then the formation of zinc vacancies. The thermal shock temperature was found to be closely related to the content of surface zinc vacancies and the photocatalytic performance. Among all our samples, the mod-ZnO-300 is the best photocatalyst owing to the highest content of surface zinc vacancies. When the thermal shock temperature overpassed 300°C, the surface zinc vacancies decreased, leading to the declined photocatalytic activity.

Disclosure statement

No potential conflict of interest was reported by the authors.

Funding

This research is funded by Vietnam National Foundation for Science and Technology Development (NAFOSTED) under grant number [104.03-2016.43].

References

[1] Kumar SG, Rao KSRK. Comparison of modification strategies towards enhanced charge carrier separation and photocatalytic degradation activity of metal oxide semiconductors (TiO_2, WO_3 and ZnO). Appl Surf Sci. 2017;391:124–148.
[2] Sushma C, Kumar SG. Advancements in the zinc oxide nanomaterials for efficient photocatalysis. Chem Pap. 2017;71:2023–2042.
[3] Qi K, Cheng B, Yu J, et al. Review on the improvement of the photocatalytic and antibacterial activities of ZnO. J Alloys Compd. 2017;727:792–820.
[4] Ong CB, Ng LY, Mohammad AW. A review of ZnO nanoparticles as solar photocatalysts: synthesis, mechanisms and applications. Renewable Sustainable Energy Rev. 2018;81:536–551.
[5] Koida T, Chichibu SF, Uedono A, et al. Correlation between the photoluminescence lifetime and defect density in bulk and epitaxial ZnO. Appl Phys Lett. 2003;82:532–534.
[6] Kong M, Li Y, Chen X, et al. Tuning the relative concentration ratio of bulk defects to surface defects in TiO_2 nanocrystals leads to high photocatalytic efficiency. J Am Chem Soc. 2011;133:16414–16417.
[7] Lv Y, Pan C, Ma X, et al. Production of visible activity and UV performance enhancement of ZnO photocatalyst via vacuum deoxidation. Appl Catal B. 2013;138:26–32.
[8] Zhang X, Qin J, Xue Y, et al. Effect of aspect ratio and surface defects on the photocatalytic activity of ZnO nanorods. Sci Rep. 2014;4(1–8):4596.
[9] Chen D, Wang Z, Ren T, et al. Influence of defects on the photocatalytic activity of ZnO. J Phys Chem C. 2014;118:15300–15307.
[10] Aggelopoulos CA, Dimitropoulos M, Govatsi A, et al. Influence of the surface-to-bulk defects ratio of ZnO and TiO_2 on their UV-mediated photocatalytic activity. Appl Catal B. 2017;205:292–301.
[11] Wang J, Wang Z, Huang B, et al. Oxygen vacancy induced band-gap narrowing and enhanced visible light photocatalytic activity of ZnO. ACS Appl Mater Interfaces. 2012;4:4024–4030.
[12] Guo MY, Ng AMC, Liu F, et al. Effect of native defects on photocatalytic properties of ZnO. J Phys Chem C. 2011;115:11095–11101.
[13] Zhang Q, Xu M, You B, et al. Oxygen vacancy-mediated ZnO nanoparticle photocatalyst for degradation of methylene blue. Appl Sci. 2018;8(1–12):353.
[14] Ischenko V, Polarz S, Grote D, et al. Zinc oxide nanoparticles with defects. Adv Funct Mater. 2005;15:1945–1954.
[15] Wang C, Wu D, Wang P, et al. Effect of oxygen vacancy on enhanced photocatalytic activity of reduced ZnO nanorod arrays. Appl Surf Sci. 2015;325:112–116.
[16] Pan L, Wang S, Mi W, et al. Undoped ZnO abundant with metal vacancies. Nano Energy. 2014;9:71–79.
[17] Kayaci F, Vempati S, Donmez I, et al. Role of zinc interstitials and oxygen vacancies of ZnO in photocatalysis: a bottom-up approach to control defect density. Nanoscale. 2014;6:10224–10234.
[18] Hao X, Wang Y, Zhou J, et al. Zinc vacancy-promoted photocatalytic activity and photostability of ZnS for efficient visible-light-driven hydrogen evolution. Appl Catal B. 2018;221:302–311.
[19] Le TK, Flahaut D, Martinez H, et al. Surface fluorination of single-phase TiO_2 by thermal shock method for enhanced UV and visible light induced photocatalytic activity. Appl Catal B. 2014;144:1–11.
[20] Le TK, Flahaut D, Martinez H, et al. Study of the effects of surface modification by thermal shock method on photocatalytic activity of TiO_2 P25. Appl Catal B. 2015;165:260–268.
[21] Patil KC, Aruna ST, Mimani T. Combustion synthesis: an update. Curr Opin Solid State Mater Sci. 2002;6:507–512.
[22] Udduttula A, Koppala S, Swamiappan S. Sol-gel combustion synthesis of nanocrystalline wollastonite by using glycine as a fuel and its *in vitro* bioactivity studies. Trans Indian Ceram Soc. 2013;72:257–260.
[23] Koppala S, Swamiappan S. Glowing combustion synthesis, characterization, and toxicity studies of Na_2CaSiO_4 powders. Mater Manuf Process. 2015;30:1476–1481.
[24] Choudhary R, Chatterjee A, Venkatraman SK, et al. Antibacterial forsterite (Mg_2SiO_4) scaffold: A promising bioceramic for load bearing applications. Bioact Mater. 2018;3:218–224.
[25] Rodriguez-Carvajal J. Recent developments of the program FULLPROF, commission of powder diffraction. IUCr Newsletter. 2001;26:12–19.

[26] Ye JD, Gu SL, Zhu SM, et al. Raman study of lattice dynamic behaviors in phosphorus-doped ZnO films. Appl Phys Lett. 2006;88((1–3)):101905.
[27] Youn CJ, Jeong TS, Han MS, et al. Optical properties of Zn-terminated ZnO bulk. J Cryst Growth. 2004; 261:526–532.
[28] Manjon FJ, Mari B, Serrano J, et al. Silent Raman modes in zinc oxide and related nitrides. J Appl Phys. 2005;97 (1–4):053516.
[29] Fonoberov AV, Balandin AA. ZnO quantum dos: physical properties and optoelectrionic applications. J Nanoelectron Optoelectron. 2006;1:19–38.
[30] Wagner CD, Riggs WM, Davis LE, et al. Handbook of X-ray photoelectron spectroscopy. Eden Prairie, MN, USA: PerkinElme; 1979. p. 88–89.
[31] Uddin MT, Nicolas Y, Olivier C, et al. Nanostructured SnO_2-ZnO heterojunction photocatalysts showing enhanced photocatalytic activity for the degradation of organic dyes. Inorg Chem. 2012;51:7764–7773.
[32] Zheng JH, Song JL, Li XJ, et al. Experimental and first-principle investigation of Cu-doped ZnO ferromagnetic powders. Cryst Res Technol. 2011;46:1143–1148.
[33] Dupin JC, Gonbeau D, Vinatier P, et al. Systematic XPS studies of metal oxides, hydroxides and peroxides. Phys Chem Chem Phys. 2000;2(6):1319–1324.
[34] Mu J, Perlmutter DD. Thermal decomposition of carbonates, carboxylates, oxalates, acetates, formates, and hydroxides. Thermochim Acta. 1981;49: 207–218.
[35] Minero C, Mariella G, Maurino V, et al. Photocatalytic transformation of organic compounds in the presence of inorganic anions. 1. Hydroxyl-mediated and direct electron-transfer reactions of phenol on a titanium dioxide–fluoride system. Langmuir. 2000; 16:2632–2641.
[36] Minero C, Mariella G, Maurino V, et al. Photocatalytic transformation of organic compounds in the presence of inorganic ions. 2. Competitive reactions of phenol and alcohols on a titanium dioxide-fluoride system. Langmuir. 2000; 16:8964–8972.